## Identification of Hit-to-Lead Ligand Molecules that Interact with G-

### Quadruplex DNA from c-Myc Oncogene Promoter Region

3	Petar M. Mitrasinovic*
4	ORCID ID: 0000-0002-0987-4893
5	Center for Biophysical and Chemical Research, Belgrade Institute of Science and Technology,
6	11060 Belgrade, Serbia
7	*Corresponding author.
8	E-mail address: pmitrasinovic.ist-belgrade.edu.rs@tech-center.com
9	Abstract
10	Targeting guanine (G)-rich DNA sequences, folded into noncanonical G-quadruplex (G4)
11	structures, by small ligand molecules is a potential strategy for gene therapy of cancer disease
12	BRACO-19 has been recently established as a unique (thermodynamically favorable and highly
13	selective) binder, being involved in the external stacking mode of interaction with a G4-DNA
14	formed in the c-Myc oncogene promoter region (Reference no. 10). Herein, hit-to-lead ligands
15	are identified using high-throughput virtual screening (HTVS). Search of the Kyoto Encyclopedia
16	of Genes and Genomes (KEGG) databases is performed using the key pharmacophore features of
17	BRACO-19. At the very outset, out of a total of 29,009 entries, 95 hits are extracted and
18	evaluated by docking them in the binding sites of G4. Then, 22 hits are chosen by observing their
19	affinity for the receptor. Consequently, 3 hit-to-lead candidates are selected on the basis of
20	structural criteria. Finally, a lead candidate structure is proposed using analog design and
21	considering both the physicochemical requirements for optimal biological activity and a variety
22	of pharmacological standpoints. Implications of the present study for experimental research are
23	discussed.
24	Key words: anti-cancer drug design, BRACO-19, c-Myc oncogene promoter, G-quadruplex
25	DNA, hit-to-lead ligand molecule

### 1. Introduction

In addition to forming various canonical duplex structures, highly dynamical DNA macromolecules are able to fold into noncanonical structures, including hairpin, triplex, G-quadruplex, and i-motif. G-quadruplexes (or G-tetraplexes) are secondary structures that form within guanine rich strands of regulatory genomic regions (human telomeres, oncogene promoter regions, immunoglobulin switch regions, ribosomal DNA, some regions of RNA). Even though G4s associate with various conformations and folding energies, and their thermodynamic stabilities are comparable to those of duplex structures, the function of G4s *in vivo* is not fully understood. G4s are hypothesized to participate in important biological phenomena, including telomere maintenance, end-capping and protection, chromosome stability, gene expression, viral integration, and recombination.<sup>1,2</sup> A relevant consequence of G-quadruplex formation in telomeric DNA is the inhibition of telomere elongation by telomerase in cancer cells.<sup>3,4</sup> An increasing number of identified G4-binding proteins means that protein/G4 interactions are associated with important cellular events. Use of small molecules for targeting G4 in order to disrupt protein/G4 recognition emerges as a potential strategy for directing anti-cancer therapy.<sup>5</sup>

G4 structures primarily consist of two or more stacked G-tetrads (or G-quartets) assembled either from a single strand of DNA in an intramolecular (backfolded) way or from two-, three-, or four DNA strands in an intermolecular way. Every single G-tetrad contains four G-G base pairs (bps) linked by Hoogsteen hydrogen bonds. G4s are more compact structures than duplex DNAs and display well-defined binding sites. Small ligand molecules are expected to be complementary in shape and charge to the biological target. The question of finding ligands that conform to the structural and physicochemical requirements for optimal biological activity is of current relevance.

A G-rich element of repeated sequences with three or four guanine residues (between - 137 and -115 bp upstream of the P1 promoter in the c-Myc oncogene) can fold in an intramolecular G4 structure (Figure 1) in order to suppress c-Myc transcription in a silenced form. This element is a potential target for down-regulation of c-Myc overexpression in tumor cells. The interactions between structurally diversified ligand molecules (with a pronounced propensity for the receptor) and the G4 were systematically investigated from physically grounded points of view. Among the highest affinity ligands, BRACO-19 (Figure 2), a pure G-

quartet binder, was established as a unique - thermodynamically favorable ligand., increasing conformational flexibility of the G4 structure through its stacking mode of interaction. <sup>10</sup> By using the pharmacophore features of BRACO-19 (Figure 2), that is, the structural features of the ligand that are recognized at a receptor site and responsible for the ligand's biological activity, a subtle in silico protocol followed by some sort of analog design is employed in this work, with the ultimate goal to determine lead candidate structure.

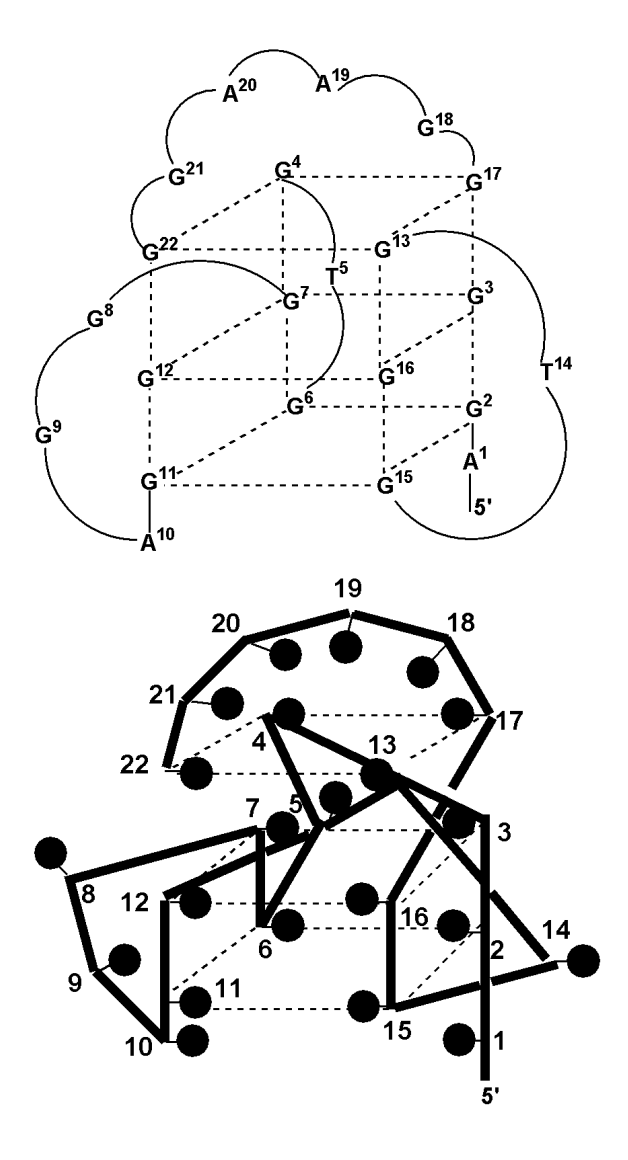


**Figure 1.** Assembly and topology of G-tetrads in G-quadruplex structure.

### 2. Methods

An experimental structure of the monomeric parallel-stranded G-quadruplex (Figure 1) was retrieved from the Research Collaboratory for Structural Bioinformatics (RCSB) Protein Data Bank (PDB) in order to obtain the initial coordinates of the target atoms (PDB ID: 2A5P).<sup>11</sup>

The term "pharmacophore" means a spatial arrangement of the essential features of an interaction. These features of BRACO-19 (Figure 2) were identified using Pharmit - an online, interactive environment for exploration of chemical space. Features supported by the interface include hydrogen bond acceptors and donors, negative and positive charges, aromatics, and hydrophobic features. For a provided ligand structure as a PDB input, the algorithm searches for these features using tolerance spheres. Structural parts of a compound match, if they can be positioned in such a way that their corresponding features are located within these spheres. Some features can have additional constraints, such as size (number of atoms) for hydrophobic features and direction for hydrogen bonds and aromatics.

Hits were generated by searching the Kyoto Encyclopedia of Genes and Genomes (KEGG) databases COMPOUND and DRUG. This search was based upon both the key pharmacophore features of BRACO-19 and SIMCOMP (SIMilar COMPound) - a graph-based method that is implemented in the KEGG system for searching and comparing chemical structures in the databases. SIMCOMP provides the atom alignments between two chemical compound graphs and calculates the similarity of two chemical compounds by counting the number of matched atoms in those atom alignments. For all calculations in SIMCOMP, the Global Search was performed and the KEGG Atom Types were chosen as a representation of atoms in order to detect biochemically meaningful features. The KEGG Atom Types are based on the chemical concept of functional groups and 68 atom types (vertex types) are defined for carbon, nitrogen, oxygen, and other atomic species with different environments. Section 16-18 All the other default options were exploited.

Virtual screening was performed for small molecules (hits) collected from KEGG against G-quadruplex DNA (PDB ID: 2A5P). A Windows platform-based graphical interface Raccoon was used for preparing and automating the AutoDock virtual screening.<sup>19</sup>

Flexible docking of each ligand (hit) in the receptor was performed by AutoDock 4.2.<sup>20,21</sup> Noteworthy is to see into why the particular method was chosen. Docking problem is an

exhaustive search problem that includes many degrees of freedom. It means that the use of efficient docking algorithms is critical for finding optimal ligand/receptor configuration and for predicting accurate binding free energy without fetching formal statistical mechanics methods. A fundamental idea underlying AutoDock 4.2 is to calculate the total ligand/receptor binding free energy by summing distinct, physically interpretable contributions.<sup>22</sup> Scoring functions are calibrated using multivariate regression analysis of a set of ligand/target receptor complexes with respect to experimentally determined structures and binding affinities. The final form of a scoring function depends on the size and quality of the training set. Since scoring functions are derived from diverse ligand/receptor complexes, possible applications are not restricted to a particular set of ligands or a specific receptor. An average level of thermochemical accuracy of 2 kcal mol<sup>-1</sup> in binding affinity predictions makes empirical scoring acceptable for the structure-based drug (or ligand) design. 23-32 The distinct energetic terms considered throughout this work account for the hydrogen bonding, the van der Waals (vdW) interactions, the electrostatic interactions, the desolvation-mediated ligand/receptor binding, the total internal energy, the torsional potential, and the unbound system's energy respectively.<sup>20</sup> Entropy of ligand interaction is reflected through the loss of degrees of freedom upon binding and is included via the torsional potential being proportional to the number of torsions (sp<sup>3</sup> bonds) in the ligand. The Lamarckian Genetic Algorithm in combination with a grid-based energy evaluation method was employed to calculate grid maps, while atomic potential grid map was computed by AutoGrid4 with a 0.536 Å spacing in a 65Å×65Å×65Å (1Å=10<sup>-10</sup>m) box centered on the macromolecule. All the other default options were chosen in the AutoDockTools4 for preparing the systems for runs.<sup>21</sup> The lowest energy and physically meaningful (in terms of the spatial orientation of a ligand with respect to the compact binding sites of G4) conformations were extracted from docking experiments. A hit affinity for the receptor was estimated by the total binding free energy ( $\Delta G_{\text{binding}}$ ) or the dissociation constant ( $K_d$ ), taking into account the relation  $\Delta G_{binding}$ =RT  $ln(K_d)$  (R=1.9872 kcal  $K^{-1}$  mol<sup>-1</sup> - the gas constant, T=300 K - the absolute temperature).

101

102

103

104

105

106

107

108

109

110

111

112

113114

115

116

117

118

119

120

121

122

123

124

125

**Figure 2.** Structure of BRACO-19 and its pharmacophore features. Each underlined atom is hydrogen bond donor (HBD) or hydrogen bond acceptor (HBA).

### 3. Results and Discussion

Ligand  $\pi$ - $\pi$  stacking at the end of G-quadruplex can be considered as a preferred mode of interaction according to experimental<sup>9,33</sup> and theoretical<sup>5,10</sup> results. Although nonspecific ligand-groove/loop binding is not inherently stable due to its dependence on a particular topology of the groove/loop,<sup>5,9</sup> the groove/loop is of interest for the structure-based drug design. This recognition motif is a viable site for blocking the interactions between G4 and its binding proteins in aqueous solution.<sup>5</sup> Search for ligands that satisfy the structural and physicochemical requirements for optimal biological activity is currently needed.

From a rigorous biophysical standpoint, the dynamics of interaction of structurally different ligand molecules with the G4 (Figure 1) was recently explored and characterized in a systematic fashion. As a consequence, the highest affinity ligands, being involved in external stacking and groove binding, were observed respectively. Interestingly, BRACO-19 (Figure 2) - a pure G-quartet binder was established to be a unique (thermodynamically favorable) ligand in terms of increasing conformational flexibility of the receptor upon external stacking. The pharmacophore of BRACO-19, which can be defined as a set of structural features in the ligand that is recognized at a receptor site and is responsible for the ligans's biological activity, is a

starting point of the present work. The particular set of structural features consists of: i) three aromatic and hydrophobic rings making the core scaffold, ii) two peripheral and hydrophobic hexagons being symmetrically attached to the core scaffold through adequate linkers, iii) three hydrogen-bond donors (HBDs), iv) five hydrogen-bond acceptors (HBAs), and v) a side chain that contains an aromatic and hydrophobic hexagon as well as a hydrophobic region on top of it (Figure 2).

KEGG database search generated hits using the pharmacophore of BRACO-19 as a template. Out of a total of 29,009 entries, 95 hits were extracted, 21 from the database Compound (Table S1, Supplementary Material) and 74 from the database Drug (Table S2, Supplementary Material). Conformations obtained by docking the hit structures in the compact binding sites of G4 were scored and affinities for G4 were evaluated.

The potency of a substance (the concentration required to achieve a defined biological effect) must be significant in order to identify a hit-to-lead. The particular concentration is in the micromolar ( $10^{-6}$  M) range for a hit and in the nanomolar ( $10^{-9}$  M) range for a lead candidate. Affinity issue can be conveniently seen through the total binding free energy ( $\Delta G_{binding}$ ) or the dissociation constant ( $K_d$ ), taking into account the relation  $\Delta G_{binding} = RT \ln(K_d)$  (R=1.9872 kcal  $K^{-1}$  mol<sup>-1</sup> - the gas constant, T=300 K – the absolute temperature). The values of  $\Delta G_{binding}$  and  $K_d$  for the BRACO-19:G4 complex, -6.77 kcal mol<sup>-1</sup> and 12.01  $\mu$ M (the footnote a of Table 1), are the references for selecting a hit that is supposed to have a higher affinity for the receptor. Thus, twenty two hits (out of the previous ninety five), which satisfy this criterion, are selected (Figure 3) and their affinity-based ranking is summarized in Table 1.

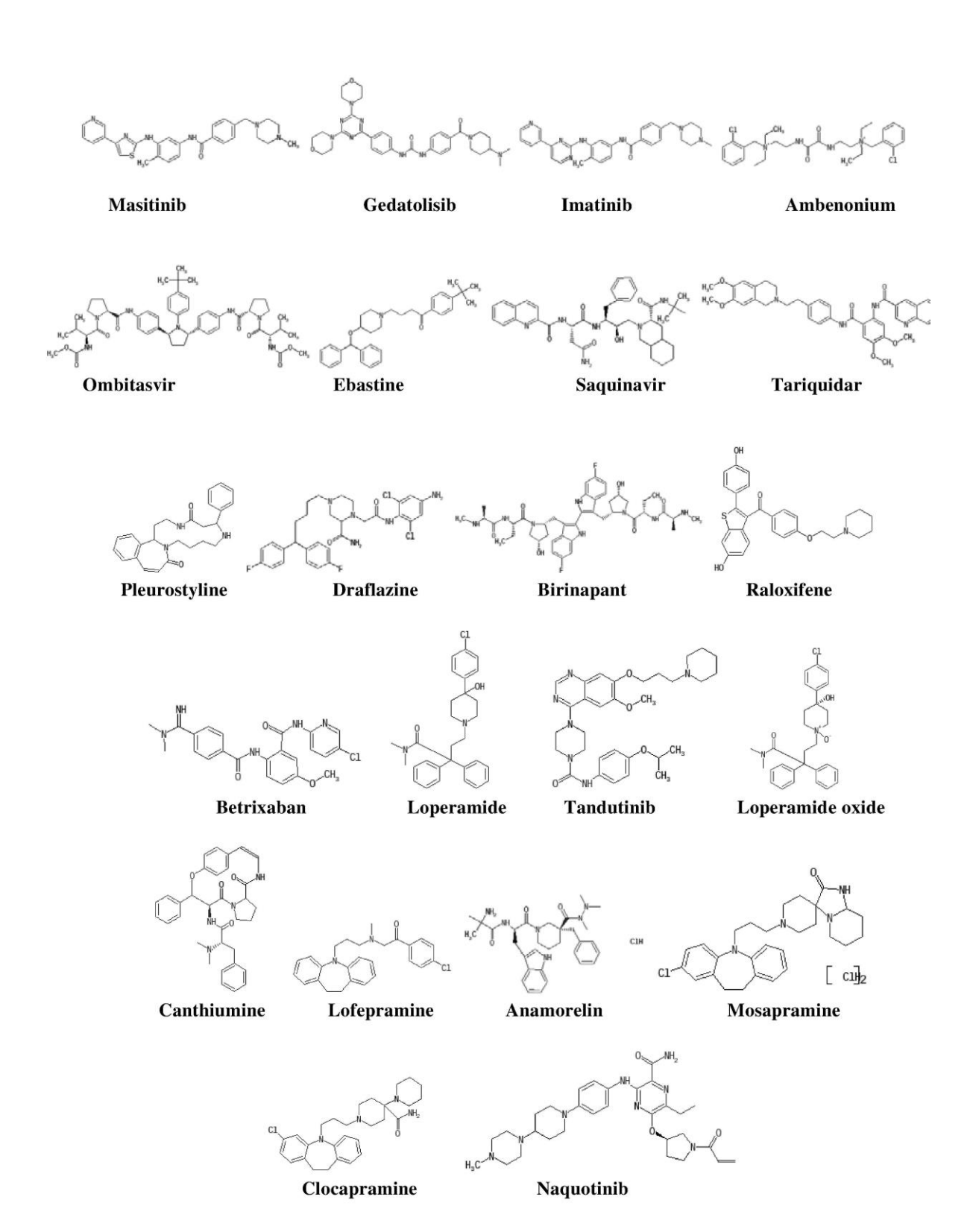


Figure 3. Structures of hit ligand molecules with the most pronounced affinity for the G4-DNA target.

Table 1. Ranking of hits according to their affinity for the G4 receptor

Ligand name <sup>(a)</sup>	$\Delta G_{ m binding}^{(b)}$	Dissociation constant <sup>(c)</sup>	$\Delta G$ intermolecular $^{(d)}$
	(kcal mol <sup>-1</sup> )	K <sub>d</sub> (μM)	(kcal mol <sup>-1</sup> )
Masitinib	-11.85	0.0021	-13.04
Gedatolisib	-10.50	0.022	-11.69
Imatinib	-10.36	0.025	-11.56
Ambenonium	-9.88	0.061	-11.07
Ombitasvir	-9.82	0.064	-11.90
Ebastine	-9.48	0.11	-10.97
Saquinavir	-9.45	0.12	-10.35
Tariquidar	-9.38	0.13	-10.87
Pleurostyline	-9.27	0.16	-9.27
Draflazine	-9.18	0.19	-9.77
Birinapant	-9.17	0.19	-10.66
Raloxifene	-8.86	0.32	-10.05
Betrixaban	-8.84	0.33	-9.73
Loperamide	-8.68	0.43	-9.57
Tandutinib	-8.52	0.57	-10.01
Loperamide oxide	-8.45	0.64	-9.05
Canthiumine	-8.45	0.64	-8.75
Anamorelin	-8.32	0.80	-9.21
Lofepramine	-8.29	0.84	-9.18
Mosapramine	-8.23	0.92	-8.53
Clocapramine	-8.21	0.95	-8.21
Naquotinib	-8.20	0.97	-9.99
	Masitinib Gedatolisib Imatinib Ambenonium Ombitasvir Ebastine Saquinavir Tariquidar Pleurostyline Draflazine Birinapant Raloxifene Betrixaban Loperamide Tandutinib Loperamide oxide Canthiumine Anamorelin Lofepramine Mosapramine Clocapramine	Masitinib -11.85 Gedatolisib -10.50 Imatinib -10.36 Ambenonium -9.88 Ombitasvir -9.82 Ebastine -9.48 Saquinavir -9.45 Tariquidar -9.38 Pleurostyline -9.27 Draflazine -9.18 Birinapant -9.17 Raloxifene -8.86 Betrixaban -8.84 Loperamide -8.68 Tandutinib -8.52 Loperamide oxide -8.45 Canthiumine -8.45 Anamorelin -8.32 Lofepramine -8.29 Mosapramine -8.23 Clocapramine -8.21	(kcal mol¹¹)         Ka (μΜ)           Masitinib         -11.85         0.0021           Gedatolisib         -10.50         0.022           Imatinib         -10.36         0.025           Ambenonium         -9.88         0.061           Ombitasvir         -9.82         0.064           Ebastine         -9.48         0.11           Saquinavir         -9.45         0.12           Tariquidar         -9.38         0.13           Pleurostyline         -9.27         0.16           Draflazine         -9.18         0.19           Birinapant         -9.17         0.19           Raloxifene         -8.86         0.32           Betrixaban         -8.84         0.33           Loperamide         -8.68         0.43           Tandutinib         -8.52         0.57           Loperamide oxide         -8.45         0.64           Canthiumine         -8.45         0.64           Anamorelin         -8.32         0.80           Lofepramine         -8.29         0.84           Mosapramine         -8.23         0.92           Clocapramine         -8.21         0.95

<sup>172 (</sup>a) Reference values for the BRACO-19:G4 complex are -6.77 kcal mol<sup>-1</sup>, 12.01 μM, and -9.99 kcal mol<sup>-1</sup> respectively.

 $<sup>173 \</sup>qquad {}^{\text{(b)}} \text{ The AutoDock 4.2 score: } \Delta G \text{binding} = E_{vdW} + E_{Hbond} + E_{desolvation} + E_{electrostatic} + E_{internal} + E_{torsional} - E_{unbound}$ 

 $<sup>174 \</sup>qquad \ ^{\text{(c)}}\Delta G_{\text{binding}} = RT \ ln(K_d), \ R - the \ gas \ constant \ (1.9872 \ kcal \ K^{-1} \ mol^{-1}), \ T - the \ absolute \ temperature \ (300 \ K), \ 1 \ \mu M = 10^{-6} \ M.$ 

 $<sup>\</sup>Delta G_{intermolecular} = E_{vdW} + E_{Hbond} + E_{desolvation} + E_{electrostatic}$ . The intermolecular energy represents the largest (most negative) contribution to the stability (binding free energy) of the complexes and does not conform to the trend displayed by the values of both  $\Delta G_{binding}$  and  $K_d$ .

The intermolecular energy (IE), also known as the interaction energy, is a key part of the enthalpy of formation of a molecular complex. In practical energetic analyses, the intermolecular energy is viewed as the largest contribution to the stability (total binding free energy) of a complex. The IE is defined as the sum of distinct energetic terms that account for the van der Waals (vdW) interactions, the hydrogen bonding, the desolvation-mediated receptor-ligand binding, and the electrostatic interactions respectively (the footnote d of Table 1). A numerical inspection of the values given in the last column of Table 1 shows that the key (negative) contribution to  $\Delta G_{\text{binding}}$  comes from the IE and that the trend of IE values does not conform to the trend displayed by the values of  $\Delta G_{\text{binding}}$  and  $K_d$  separately. The IE of the BRACO-19:G4 complex, -9.99 kcal mol<sup>-1</sup>, is a reference (the footnote a of Table 1). In comparison to the reference, the hits can be divided into two subgroups: the first one with eleven hits having the IE that is lower than the reper and the second one with the remaining hits. Thus, the members of the first subgroup are: Masitinib, Gedatolisib, Imatinib, Ambenonium, Ombitasvir, Ebastine, Saquinavir, Tariquidar, Birinapant, Raloxifene, and Tandutinib (Table 1). In other words, as far as the affinity issue is concerned, hit-to-lead candidates belong to this subgroup of hits.

In order to further filter out hit-to-lead ligands, it is necessary to invoke some structural arguments. The template structure of BRACO-19 mainly takes part in  $\pi$ - $\pi$  stacking with the  $G^2G^6G^{11}G^{15}$  tetrad by way of its core aromatic scaffold and, therefore, BRACO-19 is considered to be a G-quartet-binding ligand, even though it is involved in several, additional electrostatic interactions with the residues  $A^1$ ,  $G^6$ ,  $G^{11}$ , and  $G^{15}$  by way of its side chains. Since the interaction energy of BRACO-19 is rooted in  $\pi$ - $\pi$  stacking, any hit-to-lead candidate with a lower interaction energy is expected to be both primarily associated with external stacking of its core scaffold and more prone than BRACO-19 to electrostatic interactions via its side chain configurations. Fact that the structure of BRACO-19 contains four aromatic and hydrophobic rings (Figure 2) is employed to recruit hit-to-lead candidates from the first subgroup of hits. An inspection of the eleven hit structures (Figure 3) illustrates that Masitinib, Imatinib, and Raloxifene only have four aromatic and hydrophobic rings in the core scaffold respectively. The chemical structures of hit-to-lead candidates are shown in Figure 4.

207 Masitinib

210 Imatinib

Raloxifene

Figure 4. Structures of hit-to-lead candidates.

Knowing the structures of hit-to-lead candidates (Figure 4), the question to be raised is: what is a relevant structural basis upon which a lead candidate should rely? Besides observing individual structural and functional features of every single hit-to-lead candidate, a postulate of outstanding importance is to maintain the structural similarity between a lead candidate and a template structure (BRACO-19) as much as possible.

In contrast to Imatinib, noteworthy is that Masitinib and Raloxifene contain thiophene - a five-membered, sulfur-containing heteroaromatic ring that is often a building block in drugs

(Figure 4). Metabolism of thiophene can cause formation of reactive metabolites that may be responsible for drug-induced liver damage. Even though its presence in drugs does not necessarily result in toxic effects, thiophene is seen as a kind of structural alert. For example, tienilic acid - a thiophene-based drug was removed from the market after being both associated with severe cases of immune hepatitis and in use for only several months.<sup>36</sup> BRACO-19 does not contain a thiophene moiety (Figure 2). These observations substantiate the choice of Imatinib as a favorable hit-to-lead candidate. This choice is agreeable with the experimentally detected ability of Imatinib to downregulate telomerase activity and to inhibit proliferation in telomerase-expressing cell lines by targeting various cellular components.<sup>37</sup>

222

223

224

225

226

227

228

229

230

231

232

233

234

235

236

237

238

239

240

241

242

243

244

245

246

247

248249

250

Interesting alterations of the Imatinib structure (Figure 4) were needed in order to proceed to the proposal of a lead candidate (Figure 5). These steps were guided not only by the physicochemical requirements for optimal biological activity, but also by some sort of empirical intuition. To make the core aromatic scaffold composed of three fused aromatic rings (as that of BRACO-19, Figure 2), a carbon atom of the bottom methyl group (Figure 4) is replaced by nitrogen and an adjacent N atom is replaced by a C atom. The newly introduced N and C atoms are then bonded and the closure of the intermediate ring is achieved (Figure 5). Also, nitrogen on top of the left-hand side ring is substituted by a C atom and carbon in the central ring is replaced by an N atom (Figure 5). As for the template structure of BRACO-19 (Figure 2), two peripheral and hydrophobic hexagons that are symmetrically attached to the core scaffold through adequate linkers were shown to additionally stabilize an external stacking conformation in the stable regime of molecular dynamics simulation. <sup>10</sup> To mimic this functionality of BRACO-19, a copy of the right-hand side chain of Imatinib (Figure 4) is introduced (Figure 5) by replacing an aromatic ring (Figure 4) that is attached to the left-hand side of the core scaffold. The side chain of BRACO-19, which arises from the middle ring of the core scaffold and contains an aromatic six-membered ring (Figure 2), was found not to interact with the receptor, but its primary role in the binding conformation was to reduce deviations (or distortions) of the G-tetrad stacking portion of BRACO-19 from horizontal planarity. 10 To additionally maintain a clear resemblance of lead candidate to BRACO-19, the particular side chain (as is - without any change) is attached to the intermediate ring of the core scaffold of modified Imatinib (Figure 5).

**Figure 5.** Proposal of lead candidate structure.

252

253

254

255

256

257

258

259

260

261

262

263

264

265

266

267

268

269

270

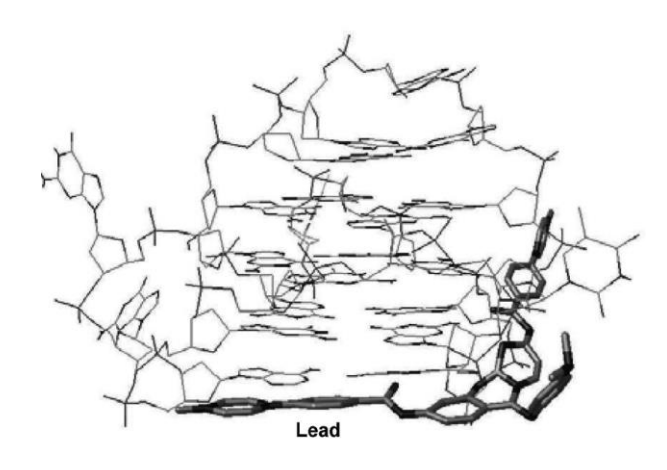
271

272

273

274

As discussed so far, virtual screening resulted in heat-to-lead candidate (Imatinib), while a transition process, from Imatinib to lead candidate, was treated as analog design. The overall protocol was initially imagined to suggest lead candidate that is able to functionally outperform BRACO-19 in binding to the G-quadruplex. To examine the extent of success of this undertaking, proposed lead candidate is docked in the target and obtained binding conformation is contrasted to that of BRACO-19 quantitatively and qualitatively. The values of  $\Delta G_{\text{binding}}$  and K<sub>d</sub> for the lead candidate:G4 complex (-11.29 kcal mol<sup>-1</sup> and 0.0053 μM) relative to those for the BRACO-19:G4 complex (-6.77 kcal mol<sup>-1</sup> and 12.01 µM) indicate a stronger affinity of the lead candidate for the receptor in comparison to the reference. A K<sub>d</sub> value of 5.3 nm conforms to the requirement of being in the nanomolar (10<sup>-9</sup> M) range that is relevant for a lead. The intermolecular energy of the lead candidate is estimated to be -13.68 kcal mol<sup>-1</sup>, which is more negative than both a corresponding value for a hit (Table 1) and that for the reference (-9.99 kcal mol<sup>-1</sup>). To rationalize the origin of a more pronounced complex stability, the mode of interaction between lead candidate and the G4 is observed with respect to the mode of interaction between BRACO-19 and the G4 (Figure 6). The simultaneous external stacking and groove binding of lead candidate has visible stabilizing advantages over the solely external stacking of BRACO-19 in forming a complex with the receptor. In this light, it is important to note the flexibility of the core structures of lead candidate and BRACO-19 (Figure 6). The flexible core scaffold of lead candidate is an advantage relative to the rigid one of BRACO-19. The conformational flexibility of small molecules proved to be more preferable compared to locking the ligands in a presumed bioactive G4 conformation.<sup>38</sup>



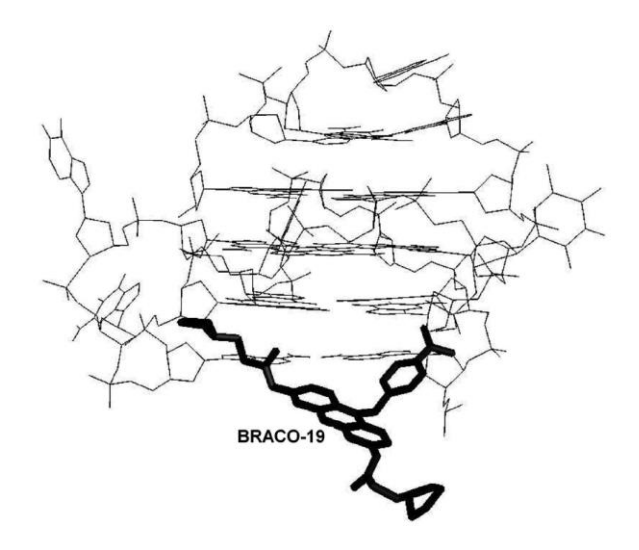


**Figure 6.** Interaction of lead candidate with G4 through external stacking and groove binding simultaneously versus external stacking of BRACO-19 with G4.

The structural design of optimal groove/loop binders is a challenge, as this mode of interaction is nonspecific and dependent on the particular topology of groove/loop residues. A pure G-quartet-binding mode is hypothesized to be more stable than a multiple-binding mode – two ligands that are involved in external stacking and loop binding respectively. A likely reason for this is that a groove/loop-binding ligand induces loop rearrangement and perturbations to the interactions between the side chains of the other G-quartet-binding ligand and the loop/groove of G-quadruplex. There are indications that a multiple-binding mode increases conformational rigidity of G-quadruplex and decreases conformational flexibility of both G-quartets and backbone. It means that such a mode of interaction, which includes two ligands, would be

thermodynamically unfavorable. The present proposal of lead candidate structure, being a Gquartet and groove/loop binder at the same time, is inclined to bypass this kind of glitch. This was accomplished using the following reasoning. Knowing that DNA-groove/ligand recognition is mainly driven by charge-induced phenomena,<sup>39-41</sup> the lead candidate was made more prone than BRACO-19 to electrostatic interactions. While the core aromatic scaffold of BRACO-19 only has one hydrogen-bond acceptor (an N atom, Figure 2), the core aromatic scaffold of lead candidate has three hydrogen-bond acceptors (three N atoms, Figure 5). While two symmetric side changes of BRACO-19 have four HBAs (two N and two O atoms) and two HBDs (two NH groups, Figure 2), two symmetric side changes of lead candidate have six HBAs (four N and two O atoms) and two HBDs (two NH groups, Figure 5). To better conceive this aspect, the mode of interaction of the lead candidate with the receptor is illustrated in Figure 7 containing a molecular surface plot with standard atom colors. The structural basis is an advance in the development of effective ligand molecules that are able to block the interactions of G4 with proteins having G4groove/loop as binding site. Taking into account both this point and the way in which the lead candidate structure was developed via analog design on top of HTVS, the lead candidate and BRACO-19 can be observed neither like clear structural nor like clear functional analogs. They should rather be placed in between structural and functional analogs.

305

288

289

290

291

292

293

294

295

296

297

298

299

300

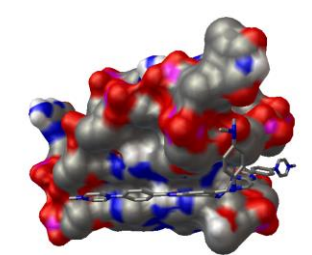
301

302

303

304

306



307308

309

310

**Figure 7.** Lead candidate is proposed to interact through external stacking and groove binding with G4 simultaneously.

311

**Table 2.** Drug likeness of lead candidate according to Lipinski's Rule of Five<sup>(a)</sup>

Ligand	Number of H-bond donors	Number of H-bond acceptors	Molecular weight (D)	LogP <sup>(b)</sup>
Lead	3	10	702.02	0
BRACO-19	3	6	550.01	2.35

<sup>(</sup>a) The Rule of Five got its name from cut-off values that are five or a multiple of five. The rule states that poor absorption or permeation is more likely when: (i) a compound has more than 5 H-bond donors (sum of OHs and NHs), (ii) there are more than 10 H-bond acceptors (sum of Ns and Os), (iii) the molecular weight is over 500 Dalton, (iv) the LogP is over 5 (or MLogP is over 4.15). 42

**Table 3.** Predictors of oral bioavailability of lead candidate according to Veber's rules<sup>(a)</sup>

Ligand	Number of torsions	Polar surface area (Ų)	Number of	Number of
		(11)	H-bond donors	H-bond acceptors
Lead	11	60.74	3	10
BRACO-19	13	9.72	3	6

<sup>(</sup>a) Based on measurements in rats for over 1,100 drug candidates, compounds that meet the following criteria may be associated with good oral bioavailability: (i) molecular flexibility reflected through 10 or fewer rotatable bonds – torsions, (ii) polar surface area equal to or less than 140 Ų, and (iii) a total number of hydrogen-bond donors and acceptors equal to or less than 12.

The correlation between the structure of a drug candidate and its oral absorption is an important point of consideration when attempting to design novel anti-cancer therapeutics. Empirical recommendations predict drug likeness on the basis of the molecular structure of drug candidate and represent useful guide in drug design process. Lipinski's rule of five (see the footnotes of Table 2)<sup>42</sup> and Veber's rules (see the footnote of Table 3)<sup>43</sup> are used to evaluate the lead candidate with respect to BRACO-19. A close inspection of the data for the lead candidate reveals that molecular weight (MW) is only out of an expected range in Table 2, while both the number of torsions and the total number of hydrogen-bond donors and acceptors are essentially lined up with the upper bounds of suggested ranges in Table 3. The MW of lead candidate is not likely to affect its good absorption as the MW of the reference (BRACO-19), being a highly selective G4-binder that is widely available on the market, is out of range as well (Table 2). An important predictor is P - an indicator of hydrophobicity and hydrophilicity. A zero value of  $\log P$  in Table 2 means that the lead candidate is equally hydrophobic and hydrophilic. This is well-

<sup>(</sup>b) Overall hydrophobicity is measured by the partition coefficient *P. P* is the water-octanol partition coefficient and is a measure of the equilibrium concentration of solute in octanol divided by the concentration of the same species in water. Log *P* is a measure of hydrophilicity/phobicity of a compound.

correlated with the polar surface area of the lead candidate (60.74 Å<sup>2</sup> in Table 3) that is roughly in middle of the expected range. In contrast, a value of 2.35 for log*P* in Table 2 means that BRACO-19 is substantially (about 224 times) more hydrophobic than hydrophilic, so that its polar surface area (9.72 Å<sup>2</sup> in Table 3) is in a close vicinity of the lower bound of the expected range. These predictions substantiate our fundamental idea to design a lead molecule that is remarkably more susceptible to charge-induced interactions with the receptor (or more specific) than BRACO-19. Further investigations correlating oral bioavailability of the particular molecule in humans and simple molecular property-based rules may be required.<sup>44</sup>

In creating a synthetic route for the development of a ligand molecule, it is necessary to create a molecular entity in which functional groups are correctly positioned in three-dimensional space; this will enable the creation of functional biophoric fragments such as the pharmacophore. The lead candidate, proposed herein, does not have chiral centers (Figure 5) and it may be eventually synthesized using the small libraries of already-prepared (e.g. by means of a split-mix approach) structural fragments (analogs),<sup>45</sup> even though a potential disadvantage of synthetic libraries is their limited structural diversity. Its atomic composition (Figure 5), presumably, does not interfere with serious side effects. The future research is supposed to see into both pharmacokinetic/dynamic and toxicity profiles *in vitro/in vivo*. We believe that this report will inspire modern organic chemists and pharmacists to face new interesting challenges of vital importance with vigor.

### 4. Conclusions

It is shown that high-throughput virtual screening in combination with analog design may be an efficient tool for identifying the chemical structure of lead candidate aimed at guiding further steps in a drug design and development process.

Substantial propensity of the lead candidate to stabilize a G-quadruplex DNA from the c-Myc oncogene promoter region is demonstrated by both satisfying the physicochemical requirements for optimal biological activity and interacting with the G4 through external stacking and groove binding simultaneously.

The results obtained in silico are a ground for the experimental analyses of pharmacokinetics/pharmacodynamics and toxicity properties *in vitro/in vivo*.

### **Supplementary Material**

- Results of the high-throughput virtual screening for hits against G-quadruplex DNA
- 372 (PDB ID: 2A5P).
- 373 **Conflict of Interest:** The author declares that he has no conflict of interest.
- 374 **References**
- 375 1. E. Ruggiero, S. N. Richter, *Nucl. Acids Res.* **2018**, *46*, 3270-3283. **DOI**:10.1093/nar/gky187
- 376 2. N. W. Luedtke, *Chimia* **2009**, *63*, 134-139. **DOI**:10.2533/chimia.2009.134
- 377 3. R. J. Harrison, J. Cuesta, G. Chessari, M. A. Read, S. K. Basra, A. P. Reszka, J. Morrell, S. M.
- Gowan, C. M. Incles, F. A. Tanious, W. D. Wilson, L. R. Kelland, S. Neidle, J. Med. Chem.
- **2003**, *46*, 4463-4476. **DOI**:10.1021/jm0308693
- 380 4. J. H. Tan, T. M. Ou, J. Q. Hou, Y. J. Lu, S. L. Huang, J. Y. Wu, Z. S. Huang, K. Y. Wong, L.
- 381 Q. Gu, J. Med. Chem. **2009**, *52*, 2825-2835. **DOI**:10.1021/jm801600m
- 382 5. J. Q. Hou, S. B. Chen, J. H. Tan, H. B. Luo, D. Li, L. Q. Gu, Z. H. Huang, *J. Comput. Aided*
- 383 *Mol. Des.* **2012**, *26*, 1355-1368. **DOI**:10.1007/s10822-012-9619-1
- 384 6. P. M. Mitrasinovic, *J. Biomol. Struct. Dyn.* **2018**, *36*, 2292-2302.
- **DOI**:10.1080/07391102.2017.1358670
- 7. D. J. Cashman, R. Buscaglia, M. W. Freyer, J. Dettler, L. H. Hurley, E. A. Lewis, J. Mol.
- 387 *Model.* **2008**, *14*, 93-101. **DOI**:10.1007/s00894-007-0254-z
- 388 8. J. Dai, M. Carver, L. H. Hurley, D. Yang, J. Am. Chem. Soc. 2011, 133, 17673-17680.
- **DOI**:10.1021/ja205646q
- 390 9. B. J. Chen, Y. L. Wu, Y. Tanaka, W. Zhang, *Int. J. Biol. Sci.* **2014**, *10*, 1084-1096.
- **DOI**:10.7150/ijbs.10190
- 392 10. P. M. Mitrasinovic, *Croat. Chem. Acta* **2019**, *92(1)*, 1-15. **DOI**:10.5562/cca3456

- 393 11. A. T. Phan, V. Kuryavyi, H. Y. Gaw, D. J. Patel, *Nat. Chem. Biol.* **2005**, *1*, 167-173.
- 394 **DOI**:10.1038/nchembio723
- 395 12. D. R. Koes, N. A. Pabon, X. Deng, M. A. Phillips, C. J. Camacho, *PLoS ONE* **2015**, *10*(8),
- 396 e0134697. **DOI**:10.1371/journal.pone.0134697
- 397 13. S. Y. Yang, *Drug Discov. Today* **2010**, *15*, 444–450. **DOI**:10.1016/j.drudis.2010.03.013
- 398 14. A. R. Leach, V. J. Gillet, R. A. Lewis, R. Taylor, *J. Med. Chem.***2010**, *53*, 539–558.
- 399 **DOI**:10.1021/jm900817u
- 400 15. J. Sunseri, D. R. Koes, *Nucl. Acids Res.* **2016**, *44*, W442–W448. **DOI**:10.1093/nar/gkw287
- 401 16. M. Hattori, N. Tanaka, M. Kanehisa, S. Goto, *Nucleic Acids Res.* **2010**, *38*, W652-W656.
- 402 **DOI**:10.1093/nar/gkq367
- 403 17. M. Hattori, Y. Okuno, S. Goto, M. Kanehisa, J. Am. Chem. Soc. 2003, 125, 11853-11865.
- 404 **DOI**:10.1021/ja036030u
- 405 18. M. Hattori, Y. Okuno, S. Goto, M. Kanehisa, *Genome Inform.* **2003**, *14*, 144-153.
- 406 **DOI**:10.11234/gi1990.14.144
- 407 19. S. Forli, R. Huey, M. E. Pique, M. F. Sanner, D. S. Goodsell, A. J. Olson, *Nat. Protoc.* **2016**,
- 408 *11(5)*, 905-919. **DOI**:10.1038/nprot.2016.051
- 409 20. G. M. Morris, D. S. Goodsell, R. S. Halliday, R. Huey, W. E. Hart, R. K. Belew, A. J. Olson,
- 410 J. Comput. Chem. **1998**, 19, 1639-1662.
- 411 **DOI**:10.1002/(SICI)1096-987X(19981115)19:14<1639::AID-JCC10>3.0.CO;2-B
- 412 21. G. M. Morris, R. Huey, W. Lindstrom, M. F. Sanner, R. K. Belew, D. S. Goodsell, A. J.
- 413 Olson, J. Comput. Chem. **2009**, 30, 2785-2791. **DOI**:10.1002/jcc.21256
- 414 22. H. J. Böhm, J. Comput. Aided Mol. Des. 1994, 8, 243–256. DOI:10.1007/BF00126743
- 415 23. P. M. Mitrasinovic, J. Comp. Chem. **2001**, 22, 1387-1395. **DOI**:10.1002/jcc.1097
- 416 24. A. D. Becke, *J. Chem. Phys.* **2002**, *117*, 6935-6938. **DOI**:10.1063/1.1503772

- 417 25. P. M. Mitrasinovic, *Chem. Phys.* **2003**, 286, 1-13. **DOI**:10.1016/S0301-0104(02)00902-3
- 418 26. A. Pavlov, P. M. Mitrasinovic, Curr. Org. Chem. 2010, 14, 129-138.
- 419 **DOI**:10.2174/138527210790069866
- 420 27. S. Cosconati, S. Forli, A. L. Perryman, R. Harris, D. S. Goodsell, A. J. Olson, *Expert Opin*.
- 421 Drug Discov. **2010**, *5*(6), 597–607. **DOI**:10.1517/17460441.2010.484460
- 422 28. B. V. Babu, N. K. Konduru, W. Nakanishi, S. Hayashi, P. M. Mitrasinovic, N. Ahmed, Anti-
- 423 Cancer Agents Med. Chem. **2013**, 13, 307-332. **DOI**:10.2174/1871520611313020017
- 424 29. P. M. Mitrasinovic, Curr. Drug. Targ. 2013, 14, 817-829.
- **DOI**:10.2174/1389450111314070009
- 426 30. P. M. Mitrasinovic, *Med. Chem.* **2014**, *10*, 252-270.
- **DOI**:10.2174/157340641003140304143442
- 428 31. P. M. Mitrasinovic, Med. Chem. 2014, 10, 46-58.
- 429 **DOI**:10.2174/157340641001131226122124
- 430 32. N. Deng, L. Wickstrom, P. Cieplak, C. Lin, D. Yang, J. Phys. Chem. B **2017**, 121(46),
- 431 10484–10497. **DOI**:10.1021/acs.jpcb.7b09406
- 432 33. S. Neidle, Curr. Opin. Struct. Biol. **2009**, 19, 239–250. **DOI**:10.1016/j.sbi.2009.04.001
- 433 34. R. Deprez-Poulain, B. Deprez, Curr. Top. Med. Chem. 2004, 4, 569-
- 434 580. **DOI**:10.2174/1568026043451168
- 435 35. M. Keseru, G. M. Makara, *Drug Discov. Today* **2006**, *11*, 741-748.
- 436 **DOI**:10.1016/j.drudis.2006.06.016
- 437 36. D. Gramec, L. P. Masic, M. S. Dolenc, *Chem. Res. Toxicol.* **2014**, 27, 1344-1358.
- 438 **DOI**:10.1021/tx500134g
- 439 37. O. Uziel, E. Fenig, J. Nordenberg, E. Beery, H. Reshef, J. Sandbank, M. Birenbaum, M.
- 440 Bakhanashvili, R. Yerushalmi, D. Luria, M. Lahav, *Br. J. Cancer* **2005**, *92*, 1881-1891.

- **DOI**: 10.1038/sj.bjc.6602592
- 38. B. Prasad, J. Jamroskovic, S. Bhowmik, R. Kumar, T. Romell, N. Sabouri, E. Chorell, *Chem.*
- 443 *Eur. J.* **2018**, *24*, 7926-7938. **DOI**:10.1002/chem.201800078
- 444 39. S. Neidle, *Nat. Prod. Rep.* **2001**, *18*, 291-309. **DOI**:10.1039/a705982e
- 445 40. P. Pandya, M. M. Islam, G. S. Kumar, B. Jayaram, S. Kumar, J. Chem. Sci. 2010, 122, 247-
- 446 257. **DOI**:10.1007/s12039-010-0029-4
- 447 41. P. M. Mitrasinovic, J. Chem. Inf. Model. **2015**, 55, 421-433. **DOI**:10.1021/ci5006965
- 448 42. C. A. Lipinski, F. Lombardo, B. W. Dominy, P. J. Feeney, Adv. Drug Delivery Rev. 2001, 46,
- 449 3-26. **DOI**:10.1016/S0169-409X(00)00129-0
- 43. D. F. Veber, S. R. Johnson, H. Y. Cheng, B. R. Smith, K. W. Ward, K. D. Kopple, J. Med.
- 451 *Chem.* **2002**, *45*, 2615-2623. **DOI**:10.1021/jm020017n
- 452 44. T. Hou, J. Wang, W. Zhang, X. Xu, J. Chem. Inf. Model. 2007, 47, 460-463.
- **DOI**:10.1021/ci6003515
- 454 45. M. Tassinari, A. Lena, E. Butovskaya, V. Pirota, M. Nadai, M. Freccero, F. Doria, S. N.
- 455 Richter, *Molecules* **2018**, *23*, 1874. **DOI:**10.3390/molecules23081874